



# Multi-scale 3D convolution feature-based Broad Learning System for Alzheimer's Disease diagnosis via MRI images

Ruizhi Han<sup>a,b</sup>, Zhulin Liu<sup>c,\*</sup>, C.L. Philip Chen<sup>c,d,b</sup>

<sup>a</sup> School of Information Science and Engineering, University of Jinan, Jinan, 250022, Shandong, China

<sup>b</sup> Faculty of Science and Technology, University of Macau, 99999, Macao Special Administrative Region of China

<sup>c</sup> School of Computer Science and Engineering, South China University of Technology, Guangzhou 510641, Guangdong, China

<sup>d</sup> Pazhou Lab, Guangzhou, 510335, Guangdong, China

## ARTICLE INFO

### Article history:

Received 5 December 2020

Received in revised form 14 February 2022

Accepted 21 February 2022

Available online 3 March 2022

### Keywords:

Alzheimer's disease

Magnetic resonance imaging

Convolutional neural network

Broad learning system

Image classification

## ABSTRACT

Alzheimer's disease (AD) has become a severe chronic disease that affects the health of the elderly all over the world. And the number of patients currently suffering continues to rise each year. With the rapid development of medical imaging technology, although researchers have done extensive works on the diagnosis of AD through new computer vision technology, it is still a challenge to realize the diagnosis of AD and Mild Cognitive Impairment (MCI) as precise as possible end-to-end by relying on Magnetic Resonance Imaging (MRI) image resources. In this paper, a new variant model of the Broad Learning System (BLS) for accurate diagnosis of AD and MCI is presented for MRI images. The proposed model is composed of two modules named feature mapping module and feature enhancement module. To adapt to the characteristics of medical images, a new feature mapping module that contains multi groups of feature down-sampling is designed to get the multi-scale features of the images without any additional feature selection. As a result, the proposed model can integrate multi-scale convolution features of the feature mapping module and abstract features of the feature enhancement module end-to-end when learning the AD diagnostic task. At the same time, the proposed model is a lightweight model whose complexity has been significantly simplified. To verify the validity of the proposed model, the ANDI-1 dataset was used in the relevant experiments. After 5-fold cross-validation, the proposed model has achieved the accuracy of 91.83% and 75.52% for the AD diagnostic task and MCI diagnostic task, respectively. The experimental results demonstrate that the proposed model could achieve better performance compared to other methods under the AD and MCI diagnostic tasks.

© 2022 Elsevier B.V. All rights reserved.

## 1. Introduction

Alzheimer's Disease (AD), the most common form of dementia, is a serious chronic disease caused by organ changes in the brain. Once AD is diagnosed, patients will suffer from it until death [1]. The mean remaining lifespan after diagnosis is approximately three to nine years [2–4]. According to the 2018 World Alzheimer report, close to 50 million people worldwide are living with dementia by 2018. And this number will triple to 152 million in 2050. Worldwide, there will be one new case of dementia every three seconds [5]. The state of AD can be divided into three categories: Alzheimer's Disease (AD), Mild Cognitive Impairment (MCI), Control Normal (CN), of which MCI can be subdivided into stable Mild Cognitive Impairment (sMCI) and progress Mild Cognitive Impairment (pMCI).

Undoubtedly, thanks to the development of medical imaging technology, more and more technical means, such as Magnetic

Resonance Imaging (MRI), Positron Emission Tomography (PET), provide effective and accurate evidence for the diagnosis of diseases. As MRI images are relatively easy to obtain (low price and short detection time) and have a higher resolution with the 3D structure, there are more MRI images than other data in clinical practice. As a result, the researchers conducted a large number of relevant studies using MRI data [6,7]. And related brain morphometric analysis using structural MRI data has been proven that it is effective in identifying anatomical differences between AD patients and normal controls, and in assessing the progression of mild cognitive impairment. As a result, more and more researchers are focusing on the diagnosis of AD by studying MRI images of patients [8–11].

Depending on the classification approach used by the researchers, the algorithms known today may be briefly divided into two categories: traditional machine learning methods and deep learning methods.

Traditional methods have done a great deal of meaningful work in finding effective feature expression. These methods usually adopt certain methods to achieve a dimensional reduction of

\* Corresponding author.

E-mail address: [liuzhl@scut.edu.cn](mailto:liuzhl@scut.edu.cn) (Z. Liu).

data or perform additional pre-processing of data. And then new features are extracted as the input of the classifier for AD classification, while the classification methods mainly adopt traditional machine learning methods such as SVM. There are two common types of cases above. The first way is to predefine multiple Regions of Interests (ROIs) [12] or coordinate points in the brain's MRI image as higher-level features or classification attentions for diagnosis. Its basic idea is that cognitive impairment is due to the changes of the brain tissue in special areas. As such, these ROI-level features attempt to model structural changes in predefined ROIs [13]. And the predefined coordination point aims to provide attention sites for the diagnosis of AD to grasp the structure changes [14]. At the same time, such approaches also aim to explore more effective ROI methods. After analyzing a variety of classical methods including Histogram of Gradients (HoG), Haar-like and Local binary patterns (LBP) and so on, [15] concluded that multi-feature fusion could obtain relatively better diagnostic results in the diagnosis of chest X-ray image-related diseases.

The second method is that the whole original brain image is taken as the feature, and relatively key features are extracted through certain dimension reduction methods for the next step of diagnosis. Principal Component Analysis (PCA) is particularly important for feature dimensionality reduction during and after feature fusion because the dimension of brain MRI images is huge if only extended, so it is commonly used [16,17]. [18] obtained the abstract features of MRI images through the fusion of 3D-HOG and PCA, and then realized the diagnosis of AD by using random forest as a classification model. Similar to the above methods, [19] constructs a complex disease diagnosis model for medical images by merging of various features and traditional methods. In addition, the 2D/3D automatic encoder is also used as a feature extractor or dimension reduction method. The model [20] constructs a convolutional auto-encoder to perform the transformation of brain MRI images from high-dimensional data to low-dimensional data and further applies SVM to complete the final AD diagnostic task.

Except for the above methods, deep learning approaches, which are proposed in the field of computer vision, are widely applied in AD diagnosis and tend to develop ensemble diagnosis methods. For the single deep learning model, numerous methods are designed for AD diagnosis, such as [21,22]. These methods provide different deep structures for performing AD diagnostic task, mainly based on multi-layer convolution. However, it also leads to a large number of model parameters and makes the model more complex, which is not conducive to actual deployment. For the ensemble model, the simplest and most efficient method is to integrate several models, which may make the model more robust and stable in performance [23–28]. With the further development of data diversity, multi-modal data (Image, Cerebrospinal Fluid(CSF), and so on.) ensemble learning are increasingly attracting attention [29–32]. Furthermore, the diagnosis of AD through multitasking joint learning was also proposed by researchers, but beyond the scope of this study [33].

For the strategy of the design model, although the above different kinds of methods have brought new ideas to the diagnosis of AD and improved the diagnostic results, they are facing inevitable challenges due to their respective limitations. For the first type, pre-defined regions of interest require additional prior knowledge, that is, additional algorithms should be applied to complete this preprocessing step. In addition, this two-stage method has no backward learning ability because the second stage is independent of the first stage. And the performance of the second stage relies heavily on the preprocessed features of the first stage. Therefore, an end-to-end method is needed to close the gap between the two stages. For the second kind, the ensemble learning methods not only need different

algorithms to obtain various features or excellent model groups but also need to develop appropriate fusion strategies for the above features or model groups to achieve better performance, in which the diagnosis process is complicated and inefficient. Medical images usually face the problem that it is difficult to label and the number of labeled images is limited. Thus, multi-modal ensemble learning with data augmentation is more expensive and challenging to achieve. As a result, improving the performance of a single model based on MRI images is still an important work that requires more attention. In addition, while ensuring the performance of the model, a more concise and lightweight model is also an important requirement in the actual deployment of the model.

It is well known that medical images are typically characterized by global similarity and local differences. With limited medical image resources, considering the global similarity and local differences in MRI images is a beneficial means that we can take into account.

Considering the above problems and practical requirements, we are committed to designing a new module combining the characteristics of global similarity and local difference of medical images, realizing the end-to-end classification, and providing a lightweight model on the premise of ensuring performance. As a consequence, a novel 3D convolutional variant algorithm based on BLS is proposed in this paper, which is for the purpose of providing a better alternative model to diagnose AD by using MRI images. Proposed by Chen et al. in 2018 [34], the BLS algorithm is a new neural network structure that contains a feature mapping module and a feature enhancement module, which is based on the Random Vector Functional-Link Neural Network (RVFLNN) [35]. With its special network structure, BLS can contribute to the classification by considering the different features of different levels. Benefit from the advantage, the model designed in this study can take both the highly abstract features obtained by the multi-layer convolution operation and the multi-scale features obtained by the underlying convolution layers into account. Therefore, the contributions in this paper can be summarized as follows:

- **New module:** A new Feature Mapping Module (FMM) for Broad Learning System (BLS) is designed based on 3D convolution to better extract the overall features of MRI images. Then the algorithm itself can take into consideration the global similarity and local difference of medical images.
- **Light-weighted:** Compared to other similar AD diagnostic algorithms and BLS homologous algorithms, the proposed model is more concise and the complexity of the model is smaller. To our knowledge, this algorithm is the first 3D model of homologous heterogeneity of the BLS algorithm based on MRI images.

This paper is mainly composed of the following parts. The introduction and contributions are given in the first section. The second section presents the dataset, data preprocessing, and the model proposed in this paper. In the third section, the proposed model and other related algorithms are combined into the experimental analysis. Finally, the summary of the full paper and future work are given in the fourth section.

## 2. Materials and methods

### 2.1. Data description

Data used in the preparation of this article were obtained from the Alzheimer's Disease Neuroimaging Initiative (ADNI) database

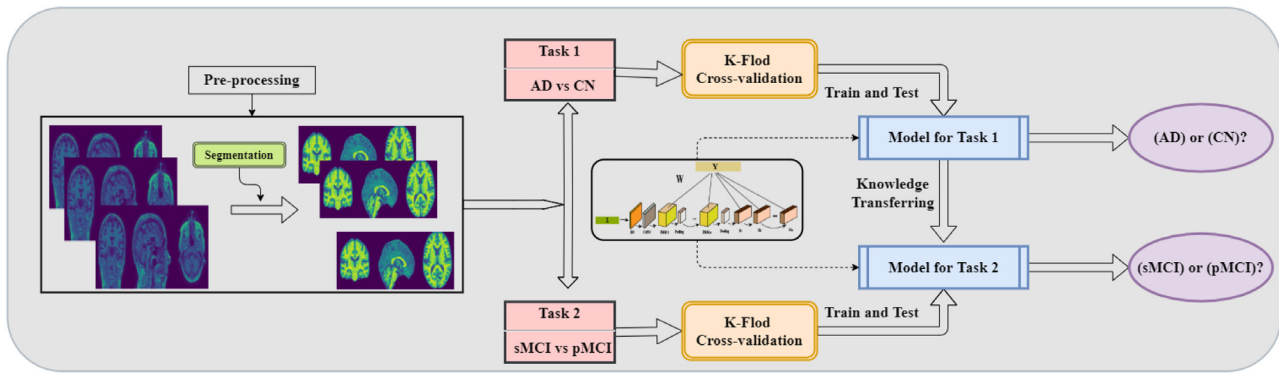


**Fig. 1.** The overall flow of AD diagnosis based on MRI images: from preprocessing of raw images to disease classification. The preprocessing operation, such as skull removal, of the original image data is currently basic and indispensable for most algorithms. In addition to the above operations, the model in this paper no longer requires any further feature preprocessing operations, thus it is an almost end-to-end diagnostic model. The preprocessed MRI image data is divided into two sub-tasks, the AD diagnosis task and the MCI diagnostic task. Among them, the model trained through the AD diagnostic task can be transferred to the MCI diagnostic task.

**Table 1**  
The demographic information about the ADNI-1 dataset used in this work.

	AD	CN	pMCI	sMCI	unMCI	SUM
Subjects' number	188	228	164	126	112	818
Age range	55–91	60–90	55–88	55–88	55–89	55–91
Males/Females	99/89	118/110	100/64	84/42	74/38	475/343

Note: unMCI means MCI converters or non-converters unknown.

(adni.loni.usc.edu). The ADNI was launched in 2003 by the National Institute on Aging (NIA), the National Institute of Biomedical Imaging and Bioengineering (NIBIB), and the Food and Drug Administration (FDA), as a 5-year public-private partnership, led by the principal investigator, Michael W. Weiner, MD. The primary goal of ADNI is to test whether serial MRI, PET, other biological markers, and clinical and neuropsychological assessments subjected to participants could be combined to measure the progression of MCI and early AD. For more details of the ADNI database, please check <http://adni.loni.usc.edu>.

The public dataset Alzheimer’s Disease Neuroimaging Initiative-1 (ADNI-1) [6] is used as the training and testing dataset in this study. It contains baseline brain MRI images from Alzheimer’s disease patients and normal control subjects. The demographic information of the study subjects is reported in Table 1. All images were downloaded in the NIfTI format after being licensed by the ADNI website: <http://adni.loni.usc.edu/> and <http://ida.loni.usc.edu/>.

**ADNI-1:** The dataset contains 818 subjects, and it mainly contains three categories named AD, CN, and MCI. Among them, MCI is subdivided into three classes according to whether it is converted to AD in a limited period (36 months), namely, progressive MCI (pMCI), stable MCI (sMCI), and unknown (unMCI). The pMCI indicates that the patient was diagnosed with MCI at the first visit, but converted to AD during a 36-month follow-up visit. In contrast, sMCI illustrates that the patient did not change from MCI to AD within 36 months. The unMCI means that some diagnostic results may have been missing during the longitudinal visits, leading to the final diagnosis being unknown. In some earlier studies, such subjects were included in the sMCI group. There is a total of 818 3D-structural MRI images used in this study, including 188 AD, 228 CN, 164 pMCI, 126 sMCI, and 112 unknown convert MCI.

## 2.2. Data preprocessing

According to the ADNI acquisition protocol [6], brain examinations were performed in 1.5T using a T1-weighted

sequence. The following preprocessing steps were considered undergone on MRI images: (1) 3D grad warp correction for geometry correction caused by gradient non-linearity [36], (2) B1 non-uniformity correction for intensity correction caused by non-uniformity [37]. These preprocessing steps help to improve the standardization among MRI images from different platforms. The above-mentioned pre-processing methods are all processed by the ADNI website, that is, the image obtained from the ADNI website has been subjected to the above-mentioned preprocessing. Fig. 2.(a) shows the expanded views of an MRI image at three viewing angles.

A further processing procedure was then performed on the downloaded images, this procedure consisting of: (1) image re-orientation; (2) cropping; (3) skull-stripping; (4) image normalization, which normalizes the image to the MNI standard space by co-registration to the MNI template [38]. MRI images were then segmented into Gray Matter (GM) and White Matter (WM) tissue probability maps. After this phase, all MR images resulted to be of size  $121 \times 145 \times 121$  voxels. Fig. 2.(b) shows the expanded views of an MRI image at three viewing angles. The whole process was performed by using the CAT12 [39] software package installed on the Matlab platform (Matlab R2016b, The MathWorks). Here, the above preprocessing operation of the original MRI image is a routine step, which is adopted by almost all classification diagnosis algorithms, but it is still a relatively important pre-sequence step.

MRI volumes were visually inspected for checking homogeneity and absence of artifacts both before and after the preprocessing step. The image representation at different stages is visible in Fig. 2.

## 2.3. Method preliminaries

Broad Learning System (BLS) model is proposed by Chen et al. [34]. The network structure of BLS is developed from that of the random vector functional-link neural network (RVFLNN), which is a special three-layer network structure proposed by Pao et al. [35]. The BLS algorithm has several variations, such as Fuzzy BLS [40], BLSReg [41], and BLSRubst [42,43]. Fig. 3 illustrates the basic model of BLS and  $\mathbf{X} \in \mathbb{R}^{N \times m}$  is the input matrix,  $N$  means the number of instances, and  $m$  means the dimension of every instance.

After concatenating the output of the feature mapping layer and enhancement layer, it can be thought as the overall input of output layer, denoted as  $\mathbf{A}$ , where  $\mathbf{A} = [\psi(\mathbf{X}\mathbf{W}_{e_i} + \beta_{e_i}) \parallel \xi(\mathbf{Z}\mathbf{W}_{h_j} + \beta_{h_j})]$ .  $\mathbf{W}_e, \beta_e$  are the weights and bias from  $\mathbf{X}$  to the feature mapping layer and  $\mathbf{W}_h, \beta_h$  connect the feature mapping layer to

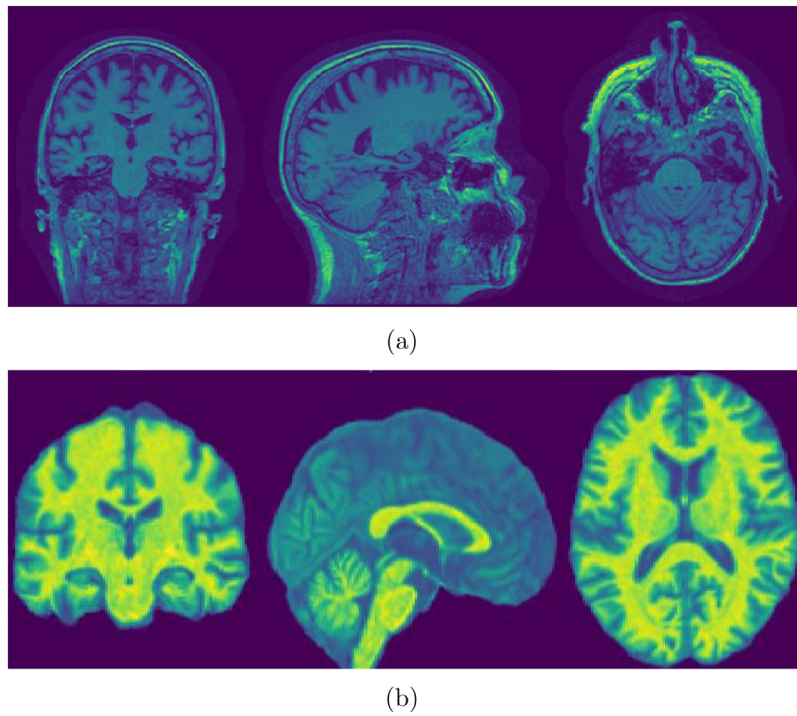


Fig. 2. Illustration of data representation: (a) Original MRI image. It should be processed by image re-orientation, cropping, skull-stripping, and image normalization. From left to right are: Coronal View, Sagittal View, and Axial View. (b) Preprocessed image. From left to right are: Coronal View, Sagittal View, and Axial View.

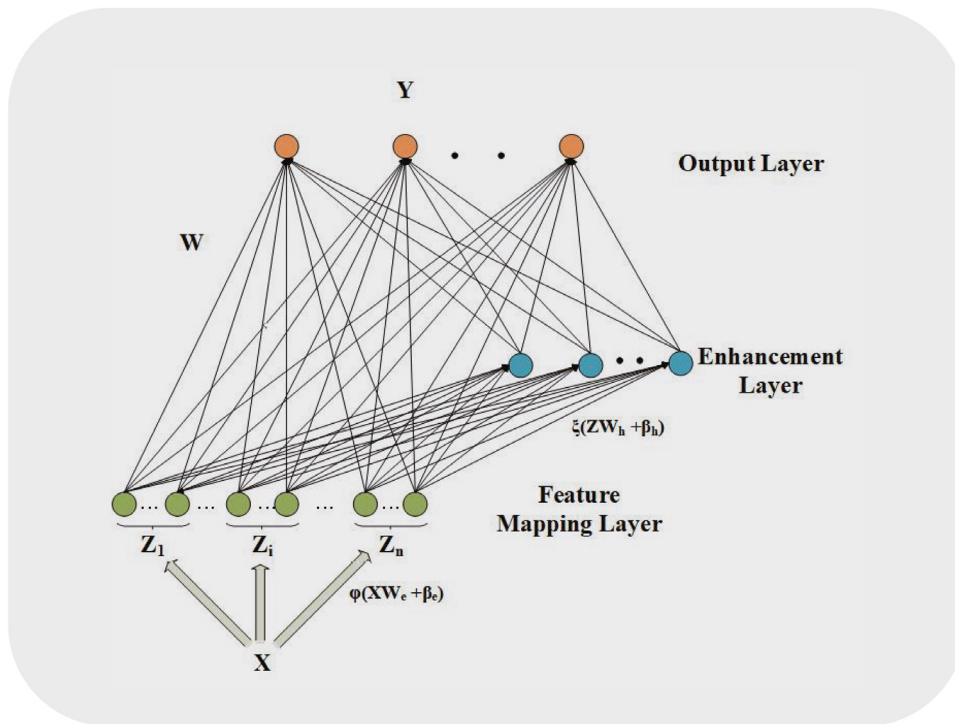


Fig. 3. Illustration of Broad Learning System: base architecture.

enhancement layer. Furthermore,  $Z$  is the output of the feature mapping layer.  $W_{e,h}$  and  $\beta_{e,h}$  are randomly generated and the dimensions of  $W_e$  and  $W_h$  are hyper-parameters.  $\psi$  and  $\xi$  are non-linear functions, such as *tansig* and *tanh*. Finally, the problem is transformed into a linear equation system problem, which is

$$AW = Y \tag{1}$$

To obtain  $W$ , Eq. (1) can be solved according to the generalized inverse and ridge regression methods by optimizing :

$$\min(\|AW - Y\|_{\rho}^{\sigma} + \lambda \|W\|_{\rho}^{\sigma}) \tag{2}$$

where  $\rho$  and  $\sigma$  always equal to 2 and  $\lambda$  is the regularization coefficient. It can be deduced that:

$$W = A^{\dagger}Y \tag{3}$$

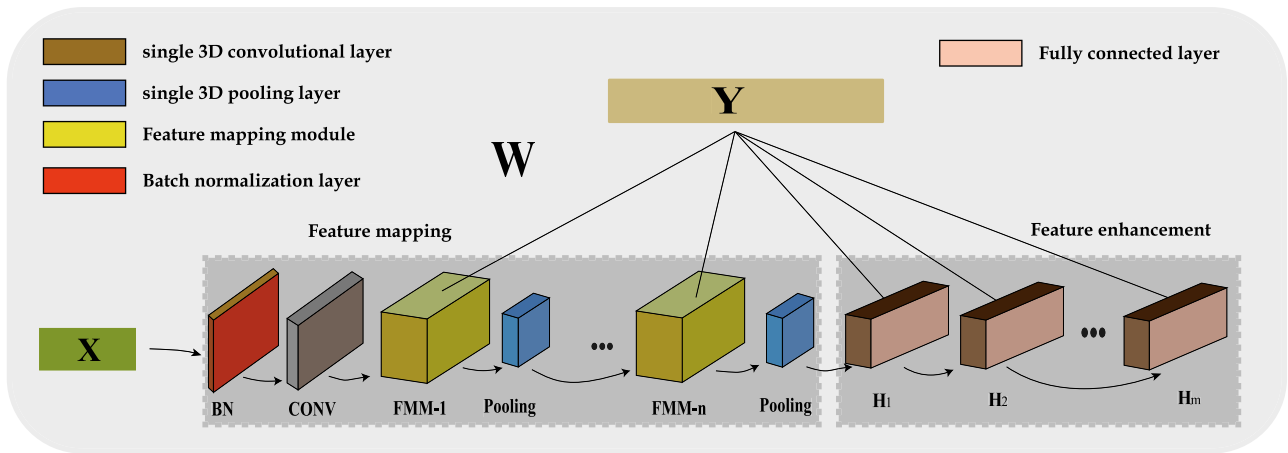


**Fig. 4.** Illustration of the proposed model. In terms of the overall structure, the model continues the classic BLS model, including two main parts. The left part of the model realizes feature mapping, and the right part functions as the feature enhancement. There are essential two aspects to the model's dataflow. The first is the horizontal transmission, which continuously obtains the data features at different granularities. The second is to pass vertically upwards, binding the various granular features obtained horizontally to the output layer ( $Y$ ) as the output weight ( $W$ ) of the model. The FMM modules (FMM-1, FMM-2, ..., FMM-n) depict the new feature mapping module and details are shown in Fig. 5. BN is the batch normalization operation, CONV and Pooling means the convolution and pooling operation, respectively. And  $H_1, H_2, \dots, H_m$  illustrate the enhancement module, which are fully connected layers.

where

$$\mathbf{A}^\dagger = \lim_{\lambda \rightarrow 0} (\lambda \mathbf{I} + \mathbf{A}\mathbf{A}^T) \mathbf{A}^T \quad (4)$$

### 3. Proposed model

The model proposed in this paper is based on the general network structure of the BLS algorithm, that is, a new convolution feature mapping structure is used to construct the feature mapping module of the BLS model, and the numerous cascaded fully-connected layers are adopted in the enhancement feature layer.

In terms of the end-to-end model design, different from traditional machine learning, which requires additional feature extraction, the model proposed in this paper draws on the advantages of autonomous learning of deep learning and obtains abstract features of high-dimensional images through convolution operation. For the purpose of fitting the type of MRI images better, the 3D kernel convolution layer is applied in this paper. Therefore, the model is trained directly on the MRI images, which does not require additional dimensionality reduction (from 3D to 2D). As a result, the proposed model is defined as a 3D convolutional broad learning system (3D-CBLS). And this model does not need to carry out additional feature extraction or feature predefining on the image except for certain necessary preprocessing operations. The image features are extracted by training the model itself to achieve end-to-end training. The overall framework of the model and the data flow is shown in Fig. 4 and Fig. 1, respectively. As shown in Fig. 1, after necessary pre-processing such as skull removal, the original image divided by the five-fold cross-validation is transmitted directly to the model for training. The image data at this point is  $X$  in Fig. 4. The final result  $Y$  obtained in Fig. 4 is the model's final diagnostic conclusion for the patient. Here, the model completes end-to-end training and prediction on the MRI image.

Except for the end-to-end design, the primary intention of the proposed model is to diversify the underlying features of MRI images as much as possible and at the same time take the high-level abstract features of the images into account, to obtain better performance in the AD diagnosis. As shown in Fig. 4, the entire model architecture has a data flow that transverse transmit from the original image ( $X$ ) to the upper-level operations, to continuously abstract the image features. The FMM is composed

of multiple convolution-activation-pooling layers, which aim to extract multi-scale underlying convolution features. And the enhancement module on the right, denoted as  $H_1, H_2, \dots, H_m$ , are conventional multi-layer neural networks with data transmission from the former one to the latter one. Consistent with the benchmark model structure of the BLS algorithm, the outputs of the feature mapping module and feature enhancement module are directly involved in the construction of the final output weight. Among them, it is worth noting that, by drawing on the structural design experience of ResNet [44], the vertical output of the first convolutional network layer was discarded. As a result, it does not directly contribute to the final output weight and the related layer is shown as 'CONV' in Figure 4.

For the feature mapping module, inspired by the special convolution structure of InceptionNet [45], the feature mapping module designed in this paper is different from other BLS variants. The proposed feature mapping module is a pipeline with a stacked convolution network block as the mainline. An instantiated feature mapping module is shown in Fig. 5. The dotted lines in Fig. 5 represent the horizontal forward data flow of the FMM module, corresponding to the horizontal input and output of FMM in Fig. 4. Meanwhile, the solid lines illustrate the vertical internal data flow of the FMM module that offers multi-scale features. And the green arrow represents the vertical output of the FMM module, corresponding to the direct connection weight from the module to the output  $Y$  in Fig. 4.

The lower convolutional layer of the multi-layer convolutional network will first extract appropriate features of the overall image. The design idea of FMM is to realize as diverse feature expression as possible on the convolution feature of the underlying layer. Therefore, the FMM is constructed according to the following rules. (A). Each FMM contains a number of parallel convolution modules, which only have data transmission at the bottom convolutional layer. Except that there is no data exchange between these convolution modules and details are available in Fig. 5. (B). The pooling of convolution features is an important downsampling method. Thus, in the different groups in Fig. 5, various pooling operation modes can be implemented, such as average pooling, maximum pooling, etc. (C). In addition to the above two aspects, the extension element-add operation under the same size is applied in FMM to achieve another kind of non-linear feature mapping. In practice, the element-add operation can be spanned to different FMMs on the premise that the feature

**Table 2**

The architecture of the model used in the experiment. Part 1:the whole architecture.

Layer name	Kernel	Output size
Input		121 × 145 × 121
BatchNormalization		121 × 145 × 121
Conv3D	3 × 3 × 3, /2, 16	61 × 73 × 61
FMM-1	Conv3D* Conv3D* Conv3D*	61 × 73 × 61 61 × 73 × 61 61 × 73 × 61
Pooling	2 × 2 × 2	30 × 36 × 30
FMM-2	Conv3D* Conv3D* Conv3D*	15 × 18 × 15 15 × 18 × 15 15 × 18 × 15
Pooling	7 × 7 × 7	2 × 2 × 2
Flatten		1 × 1 × 128
Fully Connected layers	$\begin{pmatrix} FC & 64 \\ Dropout & 0.7 \end{pmatrix} \times 5$	(1 × 1 × 64) × 5
Concatenate(FCs+Flatten)		1 × 1 × 448
Concatenate(FMMs)	Shown in Table 3	1 × 1 × 352
Concatenate(All)		1 × 1 × 800
Output		1 × 1

\* These convolutional layers are the bottom horizontal data stream convolution nodes in Fig. 6.

size is consistent. Fig. 6 illustrates an implementation of the FMM structure.

For the feature enhancement module, a multi-layer, fully connected neural network is adopted here. In Fig. 4,  $H_1, H_2, \dots, H_n$  represent a neural network with  $n$  layers of full connectivity. There is a one-way data transfer between them, and each layer contributes directly to the output layer  $Y$ . At the same time, there will be a Dropout layer to suppress the occurrence of overfitting events behind each full connection layer.

## 4. Experiment and discussion

In this section, classification experiments are applied to the ADNI-1 dataset to confirm the effectiveness of the proposed method. The evaluation of the proposed and competing methods is conducted on two binary auto diagnostic tasks: (1) AD vs. NC, (2) pMCI vs. sMCI. All experiments on the ADNI-1 dataset adopted the k-fold cross-validation method, in which K is 5 in this paper. The experimental process can be seen in Fig. 1. Here, the competing methods and the experimental settings are initially introduced.

### 4.1. Methods for comparison

In this paper, the proposed 3D-CBLS model is compared to a variety of state-of-the-art technologies, including multiple algorithms for disease diagnosis based on MRI images and the fusion of multiple data morphological features. Due to the complexity of AD-related datasets, researchers usually choose the more easily available datasets for algorithm validation. Meanwhile, the code reproduced from other published papers may not achieve the performance given in the original paper due to various limitations. This leads to the possibility of errors in the comparison of results. In order to make a more fair comparison of results, the relevant algorithms that testing on the ADNI-1 dataset were selected for the model evaluation.

**Table 3**

The architecture of the model used in the experiment. Part 2:FMM.

Layer name	Kernel	Output size	
FMM-1	$\begin{pmatrix} Conv3D^* \\ MaxPooling \\ Conv3D \\ MaxPooling \\ BN^\dagger \\ Flatten \end{pmatrix}$	$\begin{pmatrix} 3 \times 3 \times 3, 16 \\ 3 \times 3 \times 3 \\ 3 \times 3 \times 3, 8 \\ 7 \times 9 \times 7 \\ - \\ - \end{pmatrix}$	1 × 1 × 64
	$\begin{pmatrix} Conv3D^* \\ AVGPooling \\ Conv3D \\ AVGPooling \\ BN^\dagger \\ Flatten \end{pmatrix}$	$\begin{pmatrix} 3 \times 3 \times 3, 16 \\ 3 \times 3 \times 3 \\ 3 \times 3 \times 3, 8 \\ 7 \times 9 \times 7 \\ - \\ - \end{pmatrix}$	1 × 1 × 64
	$\begin{pmatrix} Conv3D^* \\ GlobalMaxPooling \end{pmatrix}$	$\begin{pmatrix} 3 \times 3 \times 3, 16 \\ - \end{pmatrix}$	1 × 1 × 16
FMM-2	$\begin{pmatrix} Conv3D^* \\ MaxPooling \\ Conv3D \\ MaxPooling \\ BN^\dagger \\ Flatten \end{pmatrix}$	$\begin{pmatrix} 3 \times 3 \times 3, 16 \\ 2 \times 2 \times 2 \\ 3 \times 3 \times 3, 8 \\ 2 \times 3 \times 2 \\ - \\ - \end{pmatrix}$	1 × 1 × 64
	$\begin{pmatrix} Conv3D^* \\ AVGPooling \\ Conv3D \\ AVGPooling \\ BN^\dagger \\ Flatten \end{pmatrix}$	$\begin{pmatrix} 3 \times 3 \times 3, 16 \\ 2 \times 2 \times 2 \\ 3 \times 3 \times 3, 8 \\ 2 \times 3 \times 2 \\ - \\ - \end{pmatrix}$	1 × 1 × 64
	$\begin{pmatrix} Conv3D^* \\ GlobalMaxPooling \end{pmatrix}$	$\begin{pmatrix} 3 \times 3 \times 3, 16 \\ - \end{pmatrix}$	1 × 1 × 16
FMMs Add Fusion	$\begin{pmatrix} Add^\dagger \\ Flatten \end{pmatrix}$	-	1 × 1 × 64
Concatenate(FMMs)		-	1 × 1 × 352

\* These layers are the same layers as the marked \* convolutional layers in Table 2.

† As these layers have the same output size, they are used as special additive fusion layers in the proposed model.

### 4.1.1. Conventional methods

As mentioned in the introduction, the models using matrix decomposition, PCA, and other statistical methods are divided into traditional conventional methods. Most of these methods require additional feature processing when making relevant diagnostics, such as the pre-delineating region of interest(ROI) or landmarks. (A). ROI-SVM and ROI-SAE [46] are both diagnosis algorithms based on ROI definition. The difference lies in that the former one (SVM) adopts PCA for feature dimension reduction, and then adopts the SVM algorithm for classification. However, based on MRI data and PET data, the latter one (SAE) is to use ROI images to train a stacked auto-encoder to reduce the feature dimension and then to diagnose AD on low-dimensional data through a full connection classification module. En-Roc [14] also adopts the method of predefining ROI to extract image ROIs in advance, and then the image is presented in a sparse manner with dimension reduction, and AD diagnosis is carried out through the Elastic network. (B). Conventional Landmark-based Morphometry (CLM) is a classification method with engineered feature representations [47]. CLM first adopts the landmarks' definition of the training set, and then performs feature extraction on that data to train an SVM classifier. On the test set, the landmarks defined in the training dataset are used to conduct SVM classification using the same feature extraction method. Similarly, based on MRI images, the CLM algorithm is used to verify the diagnosis of AD and the deterioration of MCI. However, due to different MCI datasets, the MCI diagnosis results of this article were not adopted in this paper. (C). Based on MRI data, Age data, and CM data, [48] propose an MCI diagnostic algorithm,

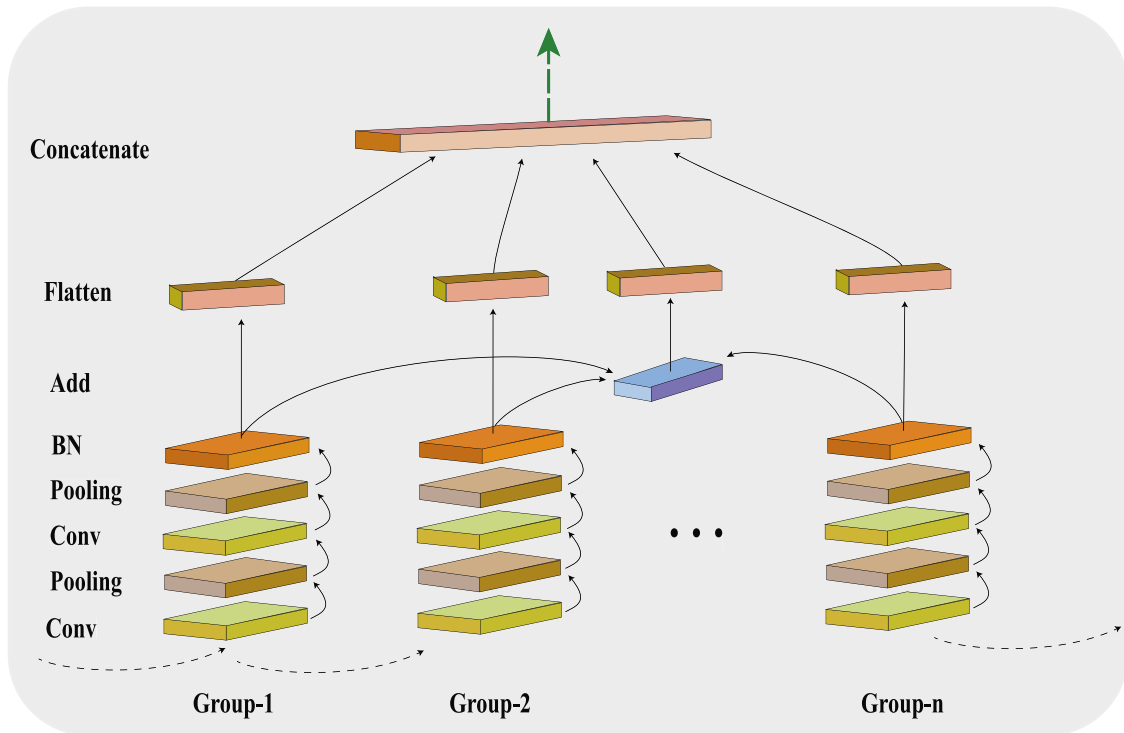


Fig. 5. Illustration of a basic feature mapping module (FMM).

which completed the classification task using SVM and LDS by combining features of various data. Among them, Cognitive Measurements (CM) data are the key information used by clinicians in diagnosis, including the Mini-Mental State Examination (MMSE), Clinical Dementia Rating (CDR), Rey Auditory Verbal Learning Test (RAVLT), Alzheimer's Disease Assessment Scale-cognitive subtest (ADAS-cog) and Functional Activities Questionnaire (FAQ), etc. For the sake of simplicity, this method simply named MCI-CP. (D). The last method involved in the comparison in this kind of method, namely LRLAD, is proposed by [31], which uses the MRI, PET, and Genetic data as a diagnostic basis. For the problem that PET and Genetic data cannot cover all subjects completely, the LRLAD algorithm adopts MRI images as routine data to extract the common latent representation, while PET images and Genetic expression as additional data to extract special latent representation. Finally, two latent representations constitute the potential space for AD classification.

#### 4.1.2. Convolutional neural networks or deep neural networks

In recent years, this method has greatly improved the diagnostic accuracy of AD by integrating various types of data. The algorithms compared in this paper mainly include the following state-of-the-art methods. (A). VCNet [21] is a deep neural network with a multi-layer convolution-activation structure stacked to realize the AD diagnosis and provide visualization of corresponding diagnosis results. (B). CAE and ICAE [22] is a set of 3D convolution classification models based on convolution auto-encoder. Similar to this paper, are dedicated to enabling end-to-end diagnosis of AD. In addition, the training strategy is similar to this paper, after the model is trained for the AD task, the knowledge is transferred to process the MCI diagnosis. The disparity between the two models is that the ICAE model borrows from the Inception model's network architecture in the model structure. (C). CMCN [49] is an ensemble learning model combining multiple convolution models, including multiple convolutional encoders and multi-layer stacked convolutional neural networks. (D). M-DeepESRNet [25] is a model constructed by another type

of ensemble learning approach. Similarly, M-DeepESRNet realized the secondary application of sparse expression features of MRI image data to the convolutional neural network through ensemble learning, namely the fusion of deep convolutional network and sparse regression model.

## 4.2. Details of the experiment

### 4.2.1. Model evaluation

For the fairness of evaluation, multiple assessment indicators were used to evaluate different models. The specific formulas can be seen as follows. Accuracy (ACC) is the overall accuracy of the outputs of the model testing on the test dataset. Sensitivity (SEN) is a measure of how well a model can correctly identify the number of positive samples in all positive samples. Similarly, specificity (SPE) is a measure of how well a model can correctly identify the number of negative samples in all negative samples. And precision refers to how many samples are correct identified in the positive samples predicted by the model. The closer its value is to 1, the better the performance of the model.

$$ACC = \frac{(TP + TN)}{(TP + TN + FP + FN)} \quad (5)$$

$$SEN = \frac{TP}{(TP + FN)} \quad (6)$$

$$SPE = \frac{TN}{(TN + FP)} \quad (7)$$

$$Precision = \frac{TP}{(TP + FP)} \quad (8)$$

Where  $TP$ ,  $TN$ ,  $FP$ ,  $FN$  is the number of true positives, true negatives, false positives, and false negatives, respectively. In addition, the commonly used classifier measurement named Area Under the Curve (AUC) in the binary classification problem, is also used in this paper.

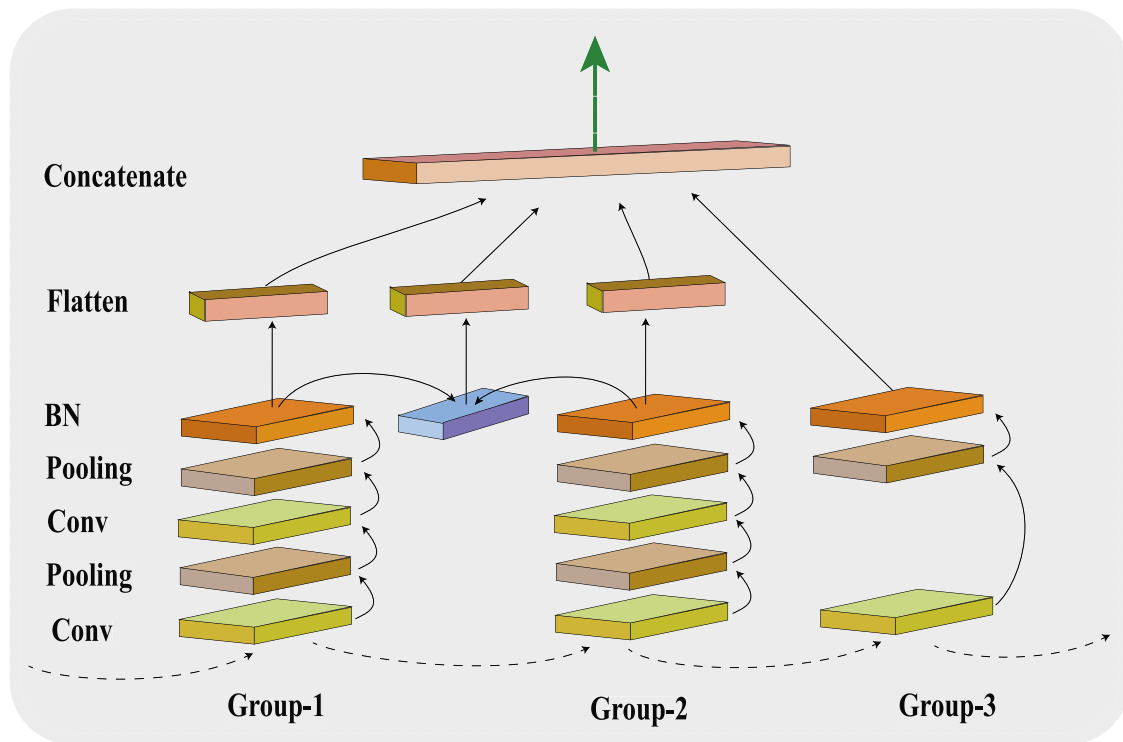


**Fig. 6.** Illustration of the feature mapping module (FMM) used in the experiment. There are three sets of convolution pooling activation modules in the module, which are G-1, G-2, and G-3 in the figure. In terms of pooling operation selection of G1, G2, and G3, this paper adopts maximum pooling, average pooling, and global maximum pooling respectively. In addition, the blue module is the element plus operation, in order to obtain more diverse features. In practice, the element plus operation can be spanned to more than one FMM if the dimensions match.

#### 4.2.2. Training strategy

As mentioned earlier, our experiment is divided into two tasks. The first is the AD diagnostic task, i.e. AD VS CN, and the second is to diagnose whether the patient is a stable MCI patient or a more severe progressive MCI, i.e. sMCI VS pMCI. For these two tasks, there are some differences in the training strategies. For the first task, the conventional method of initial training was adopted. Meanwhile, the method of 5-fold cross-validation was adopted on the dataset, and the final experimental results were obtained from the mean value of five experiments.

In recent years, transfer learning has become a learning and training method widely used by researchers. Its definition perfectly explains its main idea: the ability of a system to recognize and apply the knowledge and skills learned in previous domains/tasks to novel domains/tasks. From harm to patients, the sMCI to a certain extent can be thought of as the normal CN, and the pMCI can be thought of as the inevitable AD patients. Therefore, the second task is a more detailed and difficult sub-task of the first task in this paper. As a result, the method of transfer learning in training is adopted in this task, that is to say, the second task model at the beginning of the training will inherit the knowledge learned in the first task.

#### 4.2.3. Details of the model architecture and training settings

As well as the specific parameter details of the model, including the size of the convolution kernel, are presented in Table 2 and Table 3. In terms of the overall structure, there are two sets of FMM modules in the feature mapping module and 5 fully connected layers in the feature enhancement module. Except the final output layer adopts the *sigmoid* activation function, *ReLU* is used for all other layers requiring output activation. The learning rate is  $LR = 5e-4$ , while the probability of dropout is set to  $P = 0.7$ . Furthermore, all the kernels are initialized by 'TruncatedNormal' method, and the initialization parameters of 'TruncatedNormal'

are fixed as  $mean=0$  and  $stddev=0.05$ . And the cross-entropy loss function is adopted as the training loss function similar to other convolution algorithms. To ensure the fairness of the experimental results, the data enhancement technology is not adopted, but the image resources are normalized.

#### 4.3. Performance on ADNI-1 dataset: AD vs CN

As described in the previous section, the effectiveness of the proposed model is verified in diagnosing AD on the ADNI-1 dataset. Limited to the size of the ADNI-1 dataset, in order to evaluate the model more fairly and equitably, the k-fold cross-verification is a more reliable method.

Table 6 shows the performance of the proposed model and other models testing on the ADNI-1 dataset. By comparing the experimental results in Table 6, it can be found that this proposed model has certain comparative advantages in multiple indicators on the task of AD vs CN. Among them, the accuracy and specificity can reach the best results in all the models that provide corresponding results, especially the specificity has an obvious advantage over other models. Fig. 7 illustrates the performance of the eight models, and these results are distributed in three-dimensional coordinates according to the three indicators of ACC, SEN, and SPE.

On the one hand, compared with traditional learning methods, the proposed model has noticeable advantages in all indicators, whether it is the overall accuracy or the specificity and sensitivity to measure the accuracy of positive and negative samples. In terms of overall accuracy, the accuracy of the model in this work can reach 91.83% which performs better than other traditional methods. At the same time, the results of the proposed model still have more prominent advantages in terms of sensitivity and specificity, indicating that this model has higher accuracy in screening true negative and true positive patients. Specifically,

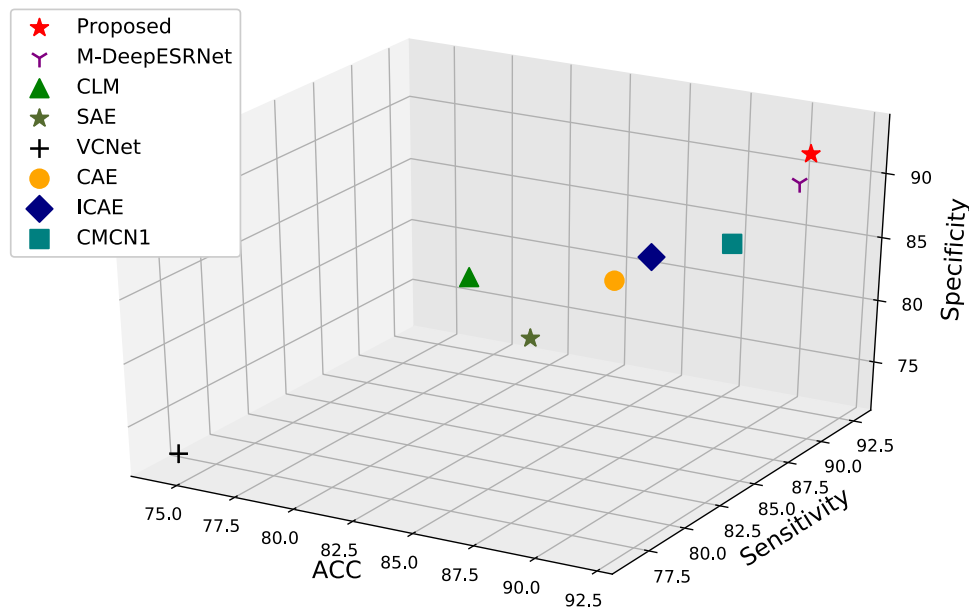


Fig. 7. Demonstration of the accuracy, specificity, and sensitivity of the eight models on the AD diagnostic task.

among all positive patients, this model can accurately screen out 90.47% of positive patients, and among all negative patients, this model can accurately screen out 93% of negative patients. These performances are significantly better than other traditional models and methods. More importantly, the proposed model does not require additional feature processing operations, such as describing the target region of interest (ROI), although it is well known that adding additional feature processing will improve the performance of the algorithm to some extent.

On the other hand, compared with these similar 3D convolution models, the model in this paper still has advantages in most evaluation indicators, except for specificity. As shown in Table 6, the accuracy of the proposed model can also reach 91.83%, which is 1.55% higher than that of the M-DeepESRNet model. However, the sensitivity of the proposed model is lower than that of the M-DeepESRNet and CMCN1 models, and the specificity is higher than them. This shows that the M-DeepESRNet and CMCN1 models have advantages in diagnosing positive patients, and the model in this paper is more reliable in diagnosing negative patients. Although the above models have their own advantages, in addition to the proposed model and the VCNet model, the other 3D convolution models require a certain degree of additional operations. For example, the CAE and ICAE models require unsupervised data pre-training, while the M-DeepESRNet model requires ensemble learning of complex models.

#### 4.4. Performance on ADNI-1 dataset by transfer learning: sMCI vs pMCI

The diagnosis of mild cognitive impairment can be viewed as a subtask of the AD diagnostic task, which is more difficult. It is generally believed that the experience gained from the diagnosis of AD can be transferred to the diagnostic task of mild cognitive impairment.

Table 7 presents the performance results of the multi-model in the course of diagnosis of mild cognitive impairment.

On the whole, the experimental results of the proposed model are similar to those of the AD diagnostic task in each evaluation measurement: ACC, Specificity, and AUC are higher than other models but the Sensitivity is lower than the MCI-CP model. Among the traditional methods, similar to the M-DeepESRNet

model that has significantly higher Sensitivity, the ability of the MCI-CP model to screen the positive samples in all positive samples is stronger than that of other models. And the Specificity of the MCI-CP model is significantly lower than that of other models, indicating that the ability of the MCI-CP model to correctly identify the negative samples in all negative samples is weak or it is hard to identify the real negative patients. In terms of the ACC and AUC, compared with the LRLAD model, the model in this paper has an average improvement of 1.22% and 1.54%, respectively, but does not require predefining the ROIs by external methods.

Compared with other 3D-CNN models, the model proposed in this paper can outperform the CAE and ICAE models in most indicators despite the same transfer learning. With respect to the M-DeepESRNet model, the model proposed in this paper exceeds it in all evaluation indicators, although the M-DeepESRNet model is a model which uses several models to learn together.

## 5. Discussion

In this section, the following points are focused to analyze and discuss the improvement.

### 5.1. Comparison of complexity between different 3D-CNN models

In the overall evaluation of different models, it is necessary to compare the overall complexity of various 3D CNN models. The complexity of a model usually includes temporal complexity and spatial complexity [50]. Among them, the spatial complexity of the model is usually compared with the parameter scale of different models. The spatial complexity describes how many parameters this model needs to define, that is, the storage space required to store the model. And the temporal complexity of the model is generally reflected by the calculation amount of the model (Floating-point Operations, FLOPs). The temporal complexity describes the amount of calculation required for data to flow through the model once.

Here, in order to measure the model complexity of the model proposed in this paper and other similar 3D CNN models, a comparison of the model complexity is present in Table 4. At the same time, the diagnostic accuracy of each model on the

**Table 4**  
Comparison of complexity between the proposed model and part of the 3D-CNN model.

Method	ACC	# of params	FLOPs
VCNet [21,22]	74.30 ± 6.34	5324K	10.64M
CAE [22]	85.24 ± 3.97	1446K	2.90M
ICAE [22]	86.60 ± 3.66	371K	0.74M
Proposed model	<b>91.83 ± 0.90</b>	<b>81K</b>	<b>0.29M</b>

Note: To facilitate the comparison between the number of parameters and the diagnostic performance, the accuracy of the above models on the AD diagnostic task was also listed here.

**Table 5**  
Validation of the FMM.

Method	ACC	# of params
Model 1	Training failure†	40K
Model 2	72.13 ± 4.02	907K
CCF-BLS [41]	84.64 ± 2.87	3.13M
Proposed model	<b>91.83 ± 0.90</b>	<b>81K</b>

† The model cannot converge in the maximum epoch, and the output results are of no practical significance.

AD diagnostic task is also listed in Table 4 to facilitate the comprehensive comparison of model complexity and model performance. The other models are not listed here because the feature pre-extraction/processing or multi-model integration is applied to their models, which would result in little comparable. By comparing, it is obvious that among the similar 3D convolutional neural network models, the proposed model can not only achieve a high accuracy of AD diagnosis, but also the complexity of the model is significantly lower than that of other models. Meanwhile, the temporal complexity of the proposed model has similar advantages compared with other models. In detail, the proposed model contains about 25% parameters and 40% FLOPs compared to the ICAE model with 5.23% higher ACC improvement.

### 5.2. Does the FMM work?

In order to verify the effectiveness of the FMM proposed in this paper, the following two models were built for the AD diagnostic task. **Model 1:** The normal horizontal feature transfer of the FMM (the dashed line of horizontal transfer in Fig. 5) was retained, but the FMM module's contribution to the final output was canceled. And all other parameters are consistent with the model proposed in this paper. **Model 2:** The network structure of Model 2 is the same as that of Model 1, however, except for the network structure, other parameters are adjusted to find the best model. In addition, the homologous isomerism model CCF-BLS [41] is also introduced in this paper as the FMM module performance comparison model.

By comparing the experimental results of all models in Table 5, it is obvious that without the FMM, the performance of the same model will decline significantly until it fails completely. If the models of the same structure work properly, additional parameters are required and diagnostic performance is compromised. Since our model can be considered as an improved version of the CCFBLS model, the longitudinal comparison with the CCF-BLS model can better illustrate the effectiveness of FMM. The CCF-BLS model is originally designed to solve the general image recognition task. For the purpose of fitting the image shape, the convolutional kernel of CCF-BLS was extended to 3D and the 3D CCF-BLS was trained on the AD diagnostic task. From the experimental results in Table 5, the proposed model can maintain excellent superiority in terms of performance and the number of model parameters.

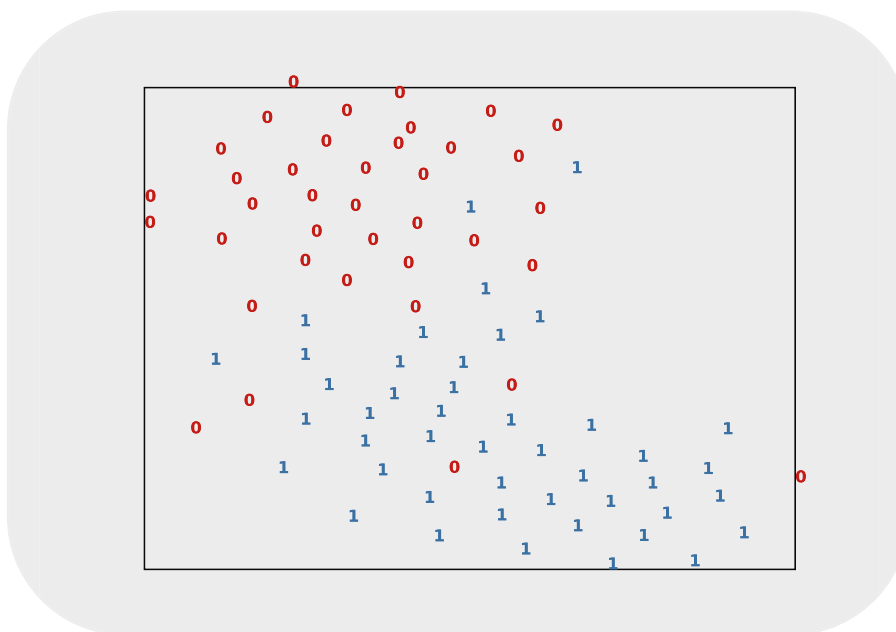
Based on the above discussion and analysis, it can be concluded that the model proposed in this paper can maintain the same level or have certain advantages as the current excellent AD diagnostic algorithm on the whole, and the scale of the model is also more concise. In addition, compared with the homology algorithm CCF-BLS, our algorithm is also an effective improved version, and as far as we know, this is the first comparison experiment on 3D medical images, and the experimental results also verify that the improved algorithm has more obvious advantages, including performance improvement and significant reduction of model size.

### 5.3. Feature visualization

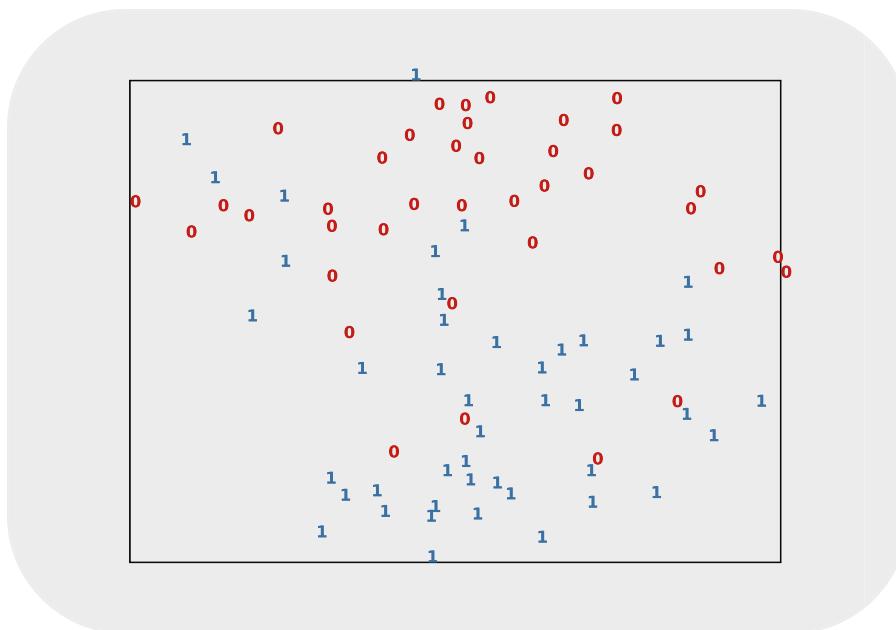
In order to show the relevant characteristics of FMM features more intuitively, the t-SNE [51] method was adopted to conduct dimensionality reduction processing for the features of different modules, so that the data distribution can be displayed. The specific content can be seen in Figure 8. Sub-figure (a) is the visualization of the top layer feature reduction of the FMM module, while sub-figure (b) is the visualization feature distribution of the feature reduction of the feature enhancement module. The red number 1s in the figure represent the same category, and the blue number 0s represent data for the other category. The data here is derived from a test set in the 5-fold cross-validation, which is predicted by the trained model of the corresponding training set. By comparing Fig. 8, it can be clearly found that the top-level feature distribution of FMM is denser than the feature enhancement module. Meanwhile, the features belonging to different classes are more distinct and almost linearly separable.

In the previous statement, it is known that medical images have obvious characteristics of global high similarity and local difference. Although higher-level abstract features strongly support classification results, low-level features are also essential to the classification task. It is well known that a stacked convolutional neural network can extract higher-level abstract features of an image and generally pay more attention to the strongest features of the classification [52,53]. And the bottom convolution will pay more attention to the texture of the image. In Fig. 4 and Fig. 5, the data flow transferred horizontally at the bottom of the proposed model is consistent with the stacked multilayer convolutional network, that is, the horizontal link at the bottom completes the work of extracting high-level abstract features. In this section, a convolution block in the FMM was extracted and traced back its final output through a gradient to obtain its attention map in the original image, and the attention map is shown in Fig. 9. At this point, the FMM completes the additional low-level feature collection. In Fig. 9, the attention map in the corresponding sub-figure (b) is in the position relation of sub-figure (a), it can be clearly found that this module can pay attention to the overall structure of the image to a certain extent, while ignoring the influence of some structures, such as the link parts of the left and right hemispheres. This can also be illustrated by the obvious difference in the output characteristics between the two modules shown in Fig. 8.

Combining the above two points, it can be concluded that FMM and Feature enhancement module have different functions for the overall model performance. FMM focuses on obtaining the underlying global features of the image. Meanwhile, combining the experimental results of models 1, 2 (with or without the FMM), and CCFBLS in Table 5, it can be proved that FMM can effectively improve the generalization performance of the model with a lightweight structure, which also proves the effectiveness of FMM.



(a)



(b)

**Fig. 8.** Illustration of data feature representation: (a) represents the feature distribution of the FMM module's top layer features reduced to two-dimensional space by the t-SNE algorithm. (b) is the feature distribution of the feature enhancement module after the same processing.

**Table 6**  
Performance of multi models on ADNI-1 dataset: AD vs CN (%).

Type	Method	Additional processing	ACC	Sensitivity	Specificity	Precision
Traditional	CLM [47]	Landmark	83.70 ± 2.60	80.90 ± 3.50	86.70 ± 2.20	-
	En-ROC [14]	ROI &Feature selection	89.10	-	-	-
	SAE [46]	ROI mark	82.59 ± 5.33	86.83 ± 6.83	77.78 ± 10.83	-
2D/3D-CNN	VCNet [21]	None	74.30 ± 6.34	76.21	72.50	-
	CAE [22]	Unsupervised pre-trained	85.24 ± 3.97	88.28	82.39	-
	ICAE [22]	Unsupervised pre-trained	86.60 ± 3.66	88.55	84.54	-
	CMCN1[49]	Ensemble learning	88.31	91.40	84.42	-
	M-DeepESRNet [25]	Ensemble learning	90.28	<b>92.65</b>	89.05	-
	Proposed model	None	<b>91.83 ± 0.90</b>	90.47 ± 3.50	<b>93.00±2.51</b>	<b>91.50±2.66</b>

Note: Values are presented as mean ± Std. The best results are marked in bold.

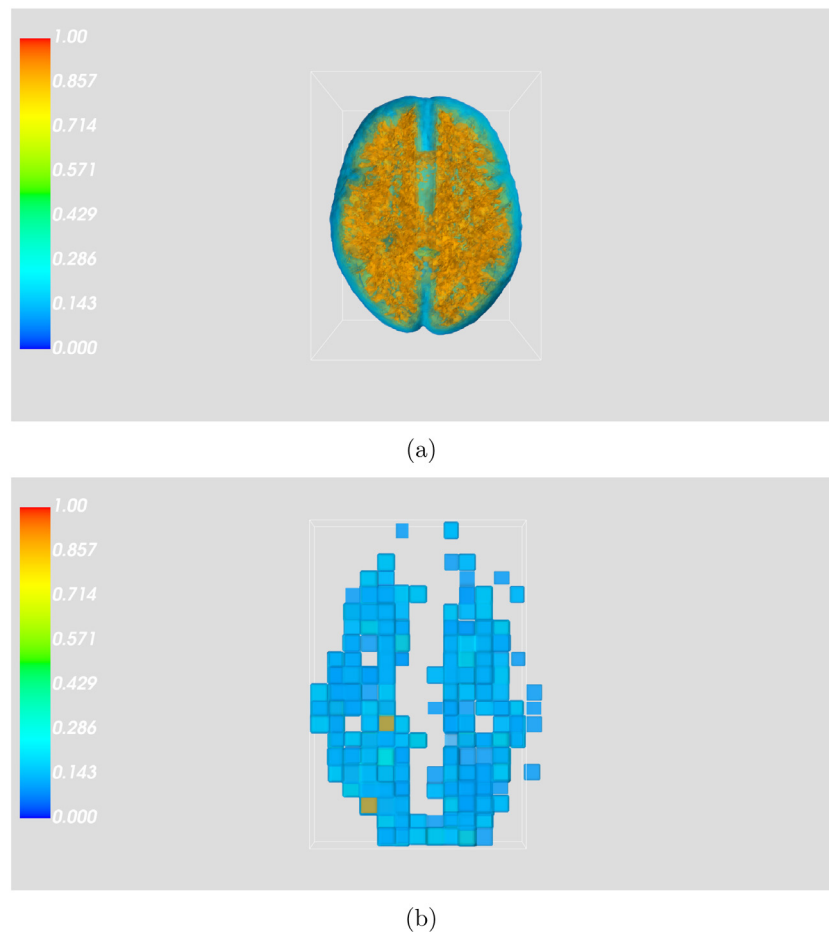


Fig. 9. Illustration of the attention map belongs to part of FMM: (a) the original brain image. (b) the feature attention map.

Table 7

Performance of multi models on ADNI-1 dataset:sMCI vs pMCI (%).

Type	Method	Additional processing	ACC	Sensitivity	Specificity	AUC
Traditional	MCI-CP [48]	Feature selection	74.74	<b>88.85</b>	51.59	76.61
	LRLAD [31]	Multi-modality&ROI	74.30	-	-	75.50
2D/3D-CNN	CAE [22]	Transfer learning	73.23 ± 4.21	74.96	71.53	-
	ICAE [22]	Transfer learning	73.95 ± 4.82	77.46	70.71	-
	M-DeepESRNet [25]	Ensemble learning	73.28 ± 6.35	70.61	75.29	71.92
	Proposed model	Transfer learning	<b>75.52 ± 2.29</b>	74.96 ± 6.06	<b>76.18 ± 8.01</b>	<b>77.04</b>

Note: Values are presented as mean ± Std. The best results are marked in bold.

## 6. Conclusion

In this paper, a novel convolution model is established for the diagnosis of AD and MCI based on MRI images. The main structure of the proposed model is derived from the Broad Learning System. On this basis, a new FMM structure is proposed to improve the BLS model and carried out experimental verification on AD medical images. This new FMM module auxiliary model completes the extraction of features of different scales and promotes the new model to achieve an improvement in the performance of the model compared with the homologous model. In terms of model learning and training, the proposed model does not require additional feature preprocessing operations and can complete model learning nearly end-to-end. Compared with some current excellent methods that require additional feature processing, such as data dimensionality reduction, feature extraction, multi models and multi types of data ensemble learning, etc., the model proposed in this paper could achieve better performance only on MRI data by relying on the model itself, which is more concise

and effective. The performance of various current excellent algorithms is tested on the ADNI-1 dataset, no matter the traditional algorithm or CNN algorithm. The testing accuracy of our model is 91.83% that 1.5% higher than that of the current best model M-DeepESRNet when diagnosing AD vs CN. Furthermore, in terms of model scale and performance, compared with other models of the same type, the most prominent advantage of the model proposed in this paper is that it takes the smallest temporal and spatial complexity to achieve the highest model diagnostic performance. For example, in the five-fold cross-validation of the ADNI-1 dataset, the performance of the proposed model on the AD diagnosis task is 1.5% higher than the average accuracy of other similar optimal models, and the number of parameters and calculations of the proposed model is at most 25% and 40% of other compared models, respectively.

In addition, the strategy of transfer learning is also applied to MCI diagnostic task by transferring the knowledge learned from the AD diagnostic task. From the experimental results, the proposed model still performs well compared with other algorithms

adopting the transfer learning strategy. At the same time, for the accuracy and AUC, the model proposed in this paper has better performance than other conventional models.

Overall, the proposed new model has a comparative performance on both the AD and MCI diagnostic tasks on the ADNI dataset with nearly end-to-end learning, light-weighted model parameters. And this paper further verified that the global feature of medical images could provide an effective auxiliary for model classification to some extent to reduce the generalization error. Therefore, in future work, we will further optimize and improve the model based on the effectiveness of the extracted features of the model itself and improve the generalization performance and anti-overfitting ability of the model, to better deal with the MCI diagnosis task.

### CRediT authorship contribution statement

**Ruizhi Han:** Methodology, Validation, Writing – original draft. **Zhulin Liu:** Conceptualization, Investigation, Writing – review & editing. **C.L. Philip Chen:** Supervision, Project administration.

### Declaration of competing interest

The authors declare that they have no known competing financial interests or personal relationships that could have appeared to influence the work reported in this paper.

### Acknowledgments

This work was funded in part by the National Key Research and Development Program of China under number 2019YFB1703600, in part by the National Natural Science Foundation of China grant under number 62006079, 61702195, 61751202, U1813203, U1801262, 61751205, in part by the China Postdoctoral Science Foundation under number 2020TQ0105, in part by the Science and Technology Major Project of Guangzhou, China under number 202007030006, in part by the Natural Science Foundation of Guangdong, China Province grant under number 2021A1515011998, in part by the Science and Technology Project of Guangzhou, China under number 202102020634, in part by The Science and Technology Development Fund, Macau SAR (File no. 0119/2018/A3).

### References

- [1] M.W. Weiner, D.P. Veitch, P.S. Aisen, L.A. Beckett, N.J. Cairns, R.C. Green, D. Harvey, C.R. Jack, W. Jagust, E. Liu, et al., The Alzheimer's disease neuroimaging initiative: a review of papers published since its inception, *Alzheimer's Dement.* 9 (5) (2013) e111–e194, URL <https://alz-journals.onlinelibrary.wiley.com/doi/full/10.1016/j.jalz.2011.09.172>.
- [2] G.M. McKhann, D.S. Knopman, H. Chertkow, B.T. Hyman, C.R. Jack Jr., C.H. Kawas, W.E. Klunk, W.J. Koroshetz, J.J. Manly, R. Mayeux, et al., The diagnosis of dementia due to Alzheimer's disease: Recommendations from the national institute on Aging-Alzheimer's association workgroups on diagnostic guidelines for Alzheimer's disease, *Alzheimer's Dement.* 7 (3) (2011) 263–269.
- [3] S. Todd, S. Barr, M. Roberts, A.P. Passmore, Survival in dementia and predictors of mortality: a review, *Int. J. Geriatr. Psychiatry* 28 (11) (2013) 1109–1124.
- [4] H.A. Fink, E.J. Linskens, P.C. Silverman, Accuracy of biomarker testing for neuropathologically defined Alzheimer disease in older adults with dementia: A systematic review, *Ann. Intern. Med.* May,19 (2020) 172:669.
- [5] C. Patterson, World Alzheimer Report 2018 the State of the Art of Dementia Research: New Frontiers, Alzheimer's Disease International (ADI), London, UK, 2018.
- [6] C.R. Jack Jr., M.A. Bernstein, N.C. Fox, P. Thompson, G. Alexander, D. Harvey, B. Borowski, P.J. Britson, J. L. Whitwell, C. Ward, et al., The Alzheimer's disease neuroimaging initiative (ADNI): MRI methods, *J. Magn. Reson. Imaging Official J. Int. Soc. Magn. Reson. Med.* 27 (4) (2008) 685–691.
- [7] C.R. Jack, R.C. Petersen, Y.C. Xu, P.C. O'Brien, G.E. Smith, R.J. Ivnik, B.F. Boeve, S.C. Waring, E.G. Tangalos, E. Kokmen, Prediction of AD with MRI-based hippocampal volume in mild cognitive impairment, *Neurology* 52 (7) (1999) 1397.
- [8] S. Basaia, F. Agosta, L. Wagner, E. Canu, G. Magnani, R. Santangelo, M. Filippi, Automated classification of alzheimer's disease and mild cognitive impairment using a single MRI and deep neural networks, *NeuroImage Clin.* 21 (2019) 101645, <http://dx.doi.org/10.1016/j.nicl.2018.101645>.
- [9] Y.R. Fung, Z. Guan, R. Kumar, J.Y. Wu, M. Fiterau, Alzheimer's disease brain MRI classification: Challenges and insights, 2019, [Cs, Eess] [arXiv: 1906.04231](https://arxiv.org/abs/1906.04231).
- [10] A.S. Lundervold, A. Lundervold, An overview of deep learning in medical imaging focusing on MRI, *Z. Medizinische Phys.* 29 (2) (2019) 102–127, <http://dx.doi.org/10.1016/j.zemedi.2018.11.002>.
- [11] G. Litjens, T. Kooi, B.E. Bejnordi, A.A.A. Setio, F. Ciampi, M. Ghafoorian, J.A.W.M. van der Laak, B. van Ginneken, C.I. Sanchez, A survey on deep learning in medical image analysis, *Med. Image Anal.* 42 (2017) 60–88, <http://dx.doi.org/10.1016/j.media.2017.07.005>, [arXiv:1702.05747](https://arxiv.org/abs/1702.05747).
- [12] R. Brinkmann, *The Art and Science of Digital Compositing: Techniques for Visual Effects, Animation and Motion Graphics*, Morgan Kaufmann, 2008.
- [13] C. Lian, M. Liu, J. Zhang, D. Shen, Hierarchical fully convolutional network for joint atrophy localization and alzheimer's disease diagnosis using structural MRI, *IEEE Trans. Pattern Anal. Mach. Intell.* 42 (4) (2020) 880–893, <http://dx.doi.org/10.1109/TPAMI.2018.2889096>.
- [14] L. Wang, Y. Liu, X. Zeng, H. Cheng, Z. Wang, Q. Wang, Region-of-interest based sparse feature learning method for Alzheimer's disease identification, *Comput. Methods Programs Biomed.* 187 (2020) 105290, <http://dx.doi.org/10.1016/j.cmpb.2019.105290>, URL <https://linkinghub.elsevier.com/retrieve/pii/S0169260719314774>.
- [15] H. Wang, M. Moradi, Y. Gur, P. Prasanna, T. Syeda-Mahmood, A multi-atlas approach to region of interest detection for medical image classification, in: M. Descoteaux, L. Maier-Hein, A. Franz, P. Jannin, D.L. Collins, S. Duchesne (Eds.), *Medical Image Computing and Computer Assisted Intervention - MICCAI 2017*, in: *Lecture Notes in Computer Science*, 2017, pp. 168–176.
- [16] C. Salvatore, A. Cerasa, P. Battista, M.C. Gilardi, A. Quattrone, I. Castiglioni, Magnetic resonance imaging biomarkers for the early diagnosis of alzheimer's disease: a machine learning approach, *Front. Neurosci.* 9 (2015) 307, URL <https://www.frontiersin.org/articles/10.3389/fnins.2015.00307/full>.
- [17] C. Salvatore, A. Cerasa, I. Castiglioni, MRI characterizes the progressive course of AD and predicts conversion to alzheimer's dementia 24 months before probable diagnosis, *Front. Aging Neurosci.* 10 (2018) URL <https://www.frontiersin.org/articles/10.3389/fnagi.2018.00135/full>.
- [18] D. Sarwinda, A. Bustamam, 3D-HOG features –based classification using MRI Images to early diagnosis of Alzheimer's disease, in: *2018 IEEE/ACIS 17th International Conference on Computer and Information Science, ICIS, 2018*, pp. 457–462.
- [19] T.V. Dittimi, C.Y. Suen, Mobile phone based ensemble classification of deep learned feature for medical image analysis, *IETE Tech. Rev.* 37 (2) (2020) 157–168.
- [20] F.J. Martinez-Murcia, A. Ortiz, J.-M. Gorriz, J. Ramirez, D. Castillo-Barnes, Studying the manifold structure of Alzheimer's disease: A deep learning approach using convolutional autoencoders, *IEEE J. Biomed. Health Inf.* 24 (1) (2020) 17–26, <http://dx.doi.org/10.1109/JBHI.2019.2914970>, URL <https://ieeexplore.ieee.org/document/8737996/>.
- [21] J. Rieke, F. Eitel, M. Weygandt, J.-D. Haynes, K. Ritter, Visualizing convolutional networks for MRI-based diagnosis of Alzheimer's disease, in: *Understanding and Interpreting Machine Learning in Medical Image Computing Applications, Workshop in MICCAI, Springer, 2018*, pp. 24–31.
- [22] K. Oh, Y.-C. Chung, K.W. Kim, W.-S. Kim, I.-S. Oh, Classification and visualization of Alzheimer's disease using volumetric convolutional neural network and transfer learning, *Sci. Rep.* 9 (1) (2019) 1–16.
- [23] J.Y. Choi, B. Lee, Combining of multiple deep networks via ensemble generalization loss, based on MRI images, for Alzheimer's disease classification, *IEEE Signal Process. Lett.* 27 (2020) 206–210, <http://dx.doi.org/10.1109/LSP.2020.2964161>.
- [24] N. An, H. Ding, J. Yang, R. Au, T.F. Ang, Deep ensemble learning for Alzheimer's disease classification, *J. Biomed. Inform.* 105 (2020) 103411, <http://dx.doi.org/10.1016/j.jbi.2020.103411>, URL <https://linkinghub.elsevier.com/retrieve/pii/S1532046420300393>.
- [25] H.-I. Suk, S.-W. Lee, D. Shen, A.D.N. Initiative, et al., Deep ensemble learning of sparse regression models for brain disease diagnosis, *Med. Image Anal.* 37 (2017) 101–113, URL <https://www.sciencedirect.com/science/article/pii/S1361841517300166?via%3Dihub>.
- [26] R. Rasti, H. Rabbani, A. Mehridehnavi, F. Hajizadeh, Macular OCT classification using a multi-scale convolutional neural network ensemble, *IEEE Trans. Med. Imaging* 37 (4) (2018) 1024–1034, <http://dx.doi.org/10.1109/TMI.2017.2780115>, URL <https://ieeexplore.ieee.org/document/8166817/>.

- [27] X. Fang, Z. Liu, M. Xu, Ensemble of deep convolutional neural networks based multi-modality images for Alzheimer's disease diagnosis, *IET Image Process.* 14 (2) (2020) 318–326, <http://dx.doi.org/10.1049/iet-ipr.2019.0617>, URL <https://digital-library.theiet.org/content/journals/10.1049/iet-ipr.2019.0617>.
- [28] M. Liu, F. Li, H. Yan, K. Wang, Y. Ma, L. Shen, M. Xu, A multi-model deep convolutional neural network for automatic hippocampus segmentation and classification in Alzheimer's disease, *NeuroImage* 208 (2020) 116459, <http://dx.doi.org/10.1016/j.neuroimage.2019.116459>, URL <https://linkinghub.elsevier.com/retrieve/pii/S105381191931050X>.
- [29] T. Tong, Q. Gao, R. Guerrero, C. Ledig, L. Chen, D. Rueckert, A.D.N. Initiative, et al., A novel grading biomarker for the prediction of conversion from mild cognitive impairment to Alzheimer's disease, *IEEE Trans. Biomed. Eng.* 64 (1) (2016) 155–165, URL <https://ieeexplore.ieee.org/document/7445862>.
- [30] C. Zhang, E. Adeli, T. Zhou, X. Chen, D. Shen, Multi-layer multi-view classification for Alzheimer's disease diagnosis, in: *Thirty-Second AAAI Conference on Artificial Intelligence*, 2018, p. 4406, URL <https://www.aaai.org/ocs/index.php/AAAI/AAAI18/paper/viewFile/16864/16751>.
- [31] T. Zhou, M. Liu, K.-H. Thung, D. Shen, Latent representation learning for Alzheimer's disease diagnosis with incomplete multi-modality neuroimaging and genetic data, *IEEE Trans. Med. Imaging* 38 (10) (2019) 2411–2422, URL <https://ieeexplore.ieee.org/document/8698846>.
- [32] L. Brand, K. Nichols, H. Wang, L. Shen, H. Huang, Joint multi-modal longitudinal regression and classification for Alzheimer's disease prediction, *IEEE Trans. Med. Imaging* 39 (6) (2020) 1845–1855, <http://dx.doi.org/10.1109/TMI.2019.2958943>, URL <https://ieeexplore.ieee.org/document/8932589>.
- [33] M. Liu, J. Zhang, E. Adeli, D. Shen, Joint classification and regression via deep multi-task multi-channel learning for Alzheimer's disease diagnosis, *IEEE Trans. Biomed. Eng.* 66 (5) (2019) 1195–1206, <http://dx.doi.org/10.1109/TBME.2018.2869989>, URL <https://ieeexplore.ieee.org/document/8463559/>.
- [34] C.P. Chen, Z. Liu, Broad learning system: an effective and efficient incremental learning system without the need for deep architecture, *IEEE Trans. Neural Netw. Learn. Syst.* 29 (1) (2018) 10–24.
- [35] Y.-H. Pao, Y. Takefujii, Functional-link net computing: theory, system architecture, and functionalities, *Computer* 25 (5) (1992) 76–79.
- [36] J. Jovicich, S. Czanner, D. Greve, E. Haley, A. van Der Kouwe, R. Gollub, D. Kennedy, F. Schmitt, G. Brown, J. MacFall, et al., Reliability in multi-site structural MRI studies: effects of gradient non-linearity correction on phantom and human data, *NeuroImage* 30 (2) (2006) 436–443.
- [37] P. Narayana, W. Brey, M. Kulkarni, C. Sievenpiper, Compensation for surface coil sensitivity variation in magnetic resonance imaging, *Magn. Reson. Imaging* 6 (3) (1988) 271–274.
- [38] G. Grabner, A.L. Janke, M.M. Budge, D. Smith, J. Pruessner, D.L. Collins, Symmetric atlas and model based segmentation: an application to the hippocampus in older adults, in: *International Conference on Medical Image Computing and Computer-Assisted Intervention*, Springer, 2006, pp. 58–66.
- [39] C. Gaser, R. Dahnke, *CAT-A Computational Anatomy Toolbox for the Analysis of Structural MRI Data*, Vol. 2016, HBM, 2016, pp. 336–348.
- [40] S. Feng, C.P. Chen, Fuzzy broad learning system: a novel neuro-fuzzy model for regression and classification, *IEEE Trans. Cybern.* 50 (2) (2020) 414–424.
- [41] C.P. Chen, Z. Liu, S. Feng, Universal approximation capability of broad learning system and its structural variations, *IEEE Trans. Neural Netw. Learn. Syst.* 30 (4) (2019) 1191–1204.
- [42] J.-W. Jin, C.P. Chen, Regularized robust broad learning system for uncertain data modeling, *Neurocomputing* 322 (2018) 58–69.
- [43] J. Jin, Z. Liu, C.P. Chen, Discriminative graph regularized broad learning system for image recognition, *Sci. China Inf. Sci.* 61 (11) (2018) 112209.
- [44] K. He, X. Zhang, S. Ren, J. Sun, Deep residual learning for image recognition, in: *Proceedings of the IEEE Conference on Computer Vision and Pattern Recognition*, 2016, pp. 770–778.
- [45] C. Szegedy, V. Vanhoucke, S. Ioffe, J. Shlens, Z. Wojna, Rethinking the inception architecture for computer vision, 2015, [Cs] [arXiv:1512.00567](https://arxiv.org/abs/1512.00567), URL <http://arxiv.org/abs/1512.00567>.
- [46] S. Liu, S. Liu, W. Cai, H. Che, S. Pujol, R. Kikinis, D. Feng, M.J. Fulham, et al., Multimodal neuroimaging feature learning for multiclass diagnosis of alzheimer's disease, *IEEE Trans. Biomed. Eng.* 62 (4) (2014) 1132–1140.
- [47] J. Zhang, Y. Gao, Y. Gao, B.C. Munsell, D. Shen, Detecting anatomical landmarks for fast Alzheimer's disease diagnosis, *IEEE Trans. Med. Imaging* 35 (12) (2016) 2524–2533, URL <https://ieeexplore.ieee.org/document/7494619>.
- [48] E. Moradi, A. Pepe, C. Gaser, H. Huttunen, J. Tohka, A.D.N. Initiative, et al., Machine learning framework for early MRI-based Alzheimer's conversion prediction in MCI subjects, *NeuroImage* 104 (2015) 398–412.
- [49] F. Li, D. Cheng, M. Liu, Alzheimer's disease classification based on combination of multi-model convolutional networks, in: *2017 IEEE International Conference on Imaging Systems and Techniques, IST, IEEE, 2017*, pp. 1–5.
- [50] P. Molchanov, S. Tyree, T. Karras, T. Aila, J. Kautz, Pruning convolutional neural networks for resource efficient inference, in: *International Conference on Learning Representations, ICLR, 2017*, [arXiv:1611.06440](https://arxiv.org/abs/1611.06440).
- [51] L.v.d. Maaten, G. Hinton, Visualizing data using t-SNE, *J. Mach. Learn. Res.* 9 (Nov) (2008) 2579–2605.
- [52] J. Gu, Z. Wang, J. Kuen, L. Ma, A. Shahroudy, B. Shuai, T. Liu, X. Wang, G. Wang, J. Cai, et al., Recent advances in convolutional neural networks, *Pattern Recognit.* 77 (2018) 354–377.
- [53] B. Zhou, A. Khosla, A. Lapedriza, A. Oliva, A. Torralba, Learning deep features for discriminative localization, in: *Proceedings of the IEEE Conference on Computer Vision and Pattern Recognition*, 2016, pp. 2921–2929, URL [http://ieeexplore.ieee.org/document/7780688](https://ieeexplore.ieee.org/document/7780688).